JOURNAL OF COMPUTATIONAL PHYSICS 100, 188–196 (1992)

Two-Dimensional Unsteady Solidification Problem Calculated by Using the Boundary-Fitted Coordinate System

M. SAITOU AND A. HIRATA

Hirata Laboratory, Department of Chemical Engineering, Waseda University, 3-4-1 Ohkubo, Shinjku-ku, Tokyo 169, Japan

Received June 7, 1990; revised March 4, 1991

Using the boundary-fitted coordinate system, we calculate the unsteady solidification problem. The model for calculation is constructed of cylindrical coordinates with a symmetrical axis. The Gauss–Seidel scheme with second-order accuracy of time and space is used as a solution method for the governing equations and the boundary-fitted coordinate system enables us to calculate the moving interface easily. The numerical results are compared with the analysis of a one-dimensional unsteady solidification problem and are in good agreement with it. From the calculations, we find a simple form of the crystal growth rate. © 1992 Academic Press, Inc.

INTRODUCTION

The vertical Bridgman technique is the very popular method by which crystals are grown from melt. Many experiments [1–5] have been done to reveal the solidification phenomena. However, many unsolved problems remain. One of them is what determines the solid–liquid interface shape and how it moves dynamically with time. The importance of the control of the interface shape has often been described [6–7]. The interface shape influences the distribution and magnitude of the thermal stress and impurities. Many numerical methods have been developed as tools for the study of the solidification problems.

Duda and his co-workers [8] proposed a kind of boundary-fitted coordinate system to calculate the moving boundary problems in the (x, y) plane. Their transformations used for the calculation were $\xi = x$ and $\eta = y/s(x, t)$, where $s(x, t)$ was the position of the interface and (ξ, η) were the coordinates of the transformed plane. Saitoh [9] used an extended version of Oberkamp's transformation [10] in radial coordinates. The finite-difference analysis was used for the calculation. Any point at which the boundary is not smooth, for example, the corner of a square, needs special consideration in his method.

Zabaras [11] provided a numerical method using the finite element methodology (FEM) for solution of the one-dimensional inverse solution problem. Albert and O'Neill [12] solved the unsteady solidification problem in the (x, y) plane using FEM. Sullivan, Lynch, and O'Neill [13] also extended their method using FEM to the planar instabilities of the solid–liquid interface. Moreover, Zabaras and Mukherjee [14] proposed a numerical method using the boundary element method (BEM) to calculate the unsteady solidification problem.

No convection driven by the buoyancy force was considered in the numerical method described above and no physical phenomena on the solid–liquid interface were found.

Crochet and his coworkers [15] calculated the unsteady melt flow during the horizontal Bridgman growth and demonstrated the oscillatory convection. Roux and Hadid [16] also calculated the unsteady convection of the horizontal Bridgman. But they had no explanation for the variation of the interface in the growth time.

We reported in previous papers [17, 18] on the steady solidification problem as a model of vertical Bridgman growth. We discussed the solution method to determine the interface shape and its position when the interface temperature was either equal or unequal to the melt temperature. In this paper, we extend the above solution method to the unsteady solidification problem and present a numerical method using the boundary-fitted coordinate system.

GOVERNING EQUATIONS

Figure 1 shows a schematic illustration of the model in cylindrical coordinates with a symmetrical axis, z. T_m, T_t, and T_b are the melting temperature, the temperature at the top of the ampoule, and the temperature at the bottom, respectively. m_L and m_S are the temperature gradients at the wall below the interface and at the wall above the interface. H_S, H_L, and W are the length of the solid, the length of the liquid, and the diameter of the solid, respectively. V_0 is the moving velocity of the temperature profile (which is equal to the crystal growth rate at $r = W/2$).

0021-9991/92 $5.00
Copyright © 1992 by Academic Press, Inc.
All rights of reproduction in any form reserved.

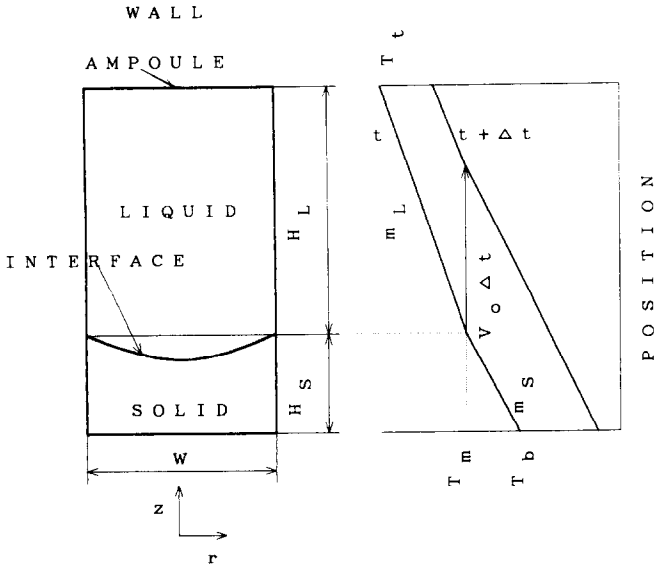

FIG. 1. Schematic illustration of the model for calculation.

Convection in the Bridgman system is driven by buoyancy differences induced by the radial and axial temperature gradients. In this system the temperature at the top wall is higher than that at the interface. That is, the axial temperature gradient operates to suppress convection. Only the radial temperature gradient causes convection in this system.

We try to calculate the equations of motion and energy in the same geometry as this study. The results show the velocity of melt is very small (for example, the maximum velocity is about 1×10^{-2} cm/s), because the radial temperature gradient is small. The convection has little effect on the interface shape. The results will be reported in detail elsewhere [19]. Therefore, the convection terms are ignored in our simplified model to obtain a basic understanding of the solidification process [7].

The governing equations in cylindrical coordinates, with the symmetrical axis z, are

$$\frac{\partial T}{\partial t}=\kappa_i\nabla^2 T, \qquad i=L,S \tag{1}$$

$$\kappa_i=k_i/\rho_i c_i,$$

$$k_S\left.\frac{\partial T}{\partial n}\right|_S=k_L\left.\frac{\partial T}{\partial n}\right|_L+\rho\,\Delta H\mathbf{v}\cdot\mathbf{n},$$

at the interface (2)

$$\frac{\partial T}{\partial r}=0, \qquad \text{at} \quad r=0, \tag{3}$$

where k_i[W/cm·K], ρ[g/cm^3], and c_i[J/g·K] are the thermal conductivity, the density, and the specific heat, respectively; $\mathbf{n}$ is the unit vector perpendicular to the solid–liquid interface, $\mathbf{v}$[cm/s] is the growth velocity vector, the subscript L or S is the abbreviation for liquid or solid and ΔH[J/g] is the latent heat.

Equation (2) is rewritten in the form derived by Crank [20],

$$g_t=(1+g_r^2)(-k_L T_z|_L+k_S T_z|_S), \tag{4}$$

where $g=g(r,t)$ is the solid–liquid interface line, g_t and g_r are the partial derivatives of $g(r,t)$ on t and on r, respectively. This form is available for calculation of the moving interface shape with time.

The boundary conditions at the side wall are given as the linear function of the temperature gradient shown in Fig. 1. For example, the temperature at the wall below the interface has the following Dirichlet type: $T=Tb+m_S z-m_S V_0 t$ at $0\leqslant z\leqslant H_S$ and at $r=W/2$, where t is the growth time.

The initial conditions for the calculation are given as both solid and liquid exist in the ampoule. Then the side walls are cooled (in Fig. 1 the temperature profile moves at the velocity, V_0), the liquid–solid interface moves and the solid grows.

We use a boundary-fitted coordinate system which is similar to the one in [17, 18] to solve the unsteady solidification problem above. The boundary-fitted coordinate system enables us to treat the moving solid–liquid interface easily and to calculate the grid points if the coordinates of the boundaries are given.

In cylindrical coordinates, the transformation equations which have the solutions of $r(\xi,\eta)$ and $z(\xi,\eta)$ are given from the results of Appendix A,

$$\begin{aligned}\alpha r_{\xi\xi}-2\beta r_{\xi\eta}+\gamma r_{\eta\eta}+Pr_\xi+Qr_\eta&=1/r,\\ \alpha z_{\xi\xi}-2\beta z_{\xi\eta}+\gamma z_{\eta\eta}+Pz_\xi+Qz_\eta&=0,\end{aligned} \tag{5}$$

$$\begin{aligned}\alpha&=(r_\eta^2+z_\eta^2)/J_0^2, \qquad \beta=(r_\xi r_\eta+z_\xi z_\eta)/J_0^2,\\ \gamma&=(r_\xi^2+z_\xi^2)/J_0^2, \qquad J_0=r_\xi z_\eta-r_\eta z_\xi.\end{aligned} \tag{6}$$

$P=P(\xi,\eta)$ and $Q=Q(\xi,\eta)$ are the space control functions which were used in [17].

Equations (1), (3), and (4) are also transformed as

$$\begin{aligned}\frac{\partial T}{\partial t}-\frac{1}{J_0}(T_\xi z_\eta-T_\eta z_\xi)\left(\frac{\partial r}{\partial t}\right)+\frac{1}{J_0}(T_\xi r_\eta-T_\eta r_\xi)\left(\frac{\partial z}{\partial t}\right),\\ =\kappa_i[\alpha T_{\xi\xi}-2\beta T_{\xi\eta}+\gamma T_{\eta\eta}+PT_\xi+QT_\eta],\end{aligned} \tag{7}$$

$$T_\xi z_\eta-T_\eta z_\xi=0, \tag{8}$$

$$g_t=(1+g_r^2)\left(-K_L\left.\frac{-r_\eta T_\xi+r_\xi T_\eta}{J_0}\right|_L+K_S\left.\frac{-r_\eta T_\xi+r_\xi T_\eta}{J_0}\right|_S\right), \tag{9}$$

where $K_i=k_i/\rho_i\,\Delta H$.

The second and third terms on the left-hand side in Eq. (7) are the moving velocity of the grid point. Through this term, the moving interface is automatically built in. So it is very easy to calculate the variation of the interface shape in time.

SOLUTION METHOD

Equation (5) is solved by the usual SOR which was used for calculating the steady solidification problem before [17]. Equation (5) means the transformation from the physical plane (r, z) to the computational plane (ξ, η). The solution method of Eq. (5) is the same as the boundary-value problem's; that is, first, the values of the boundary coordinates are given and then the quasi-elliptic equations are solved.

An iterative method with second-accurate time and space [21] is used to solve Eq. (7). The discretization is

$$\frac{T^{n+1}-T^n}{\Delta t}-\frac{1}{J_0}(T_\xi z_\eta - T_\eta z_\xi)^{n+1}\left(\frac{\partial r}{\partial t}\right)^{n+1} + \frac{1}{J_0}(T_\xi r_\eta - T_\eta r_\xi)^{n+1}\left(\frac{\partial z}{\partial t}\right)^{n+1} - \frac{\kappa_i}{2}[\alpha T_{\xi\xi} - 2\beta T_{\xi\eta} + \gamma T_{\eta\eta} + PT_\xi + QT_\eta]^{n+1} - \frac{\kappa_i}{2}[\alpha T_{\xi\xi} - 2\beta T_{\xi\eta} + \gamma T_{\eta\eta} + PT_\xi + QT_\eta]^{n} = 0. \quad (10)$$

This form corresponds to Crank–Nicolson's. An iterative solution method in this study is described below. The unknown variable $T_{i,j}^{n+1}$ is represented as T_u. Equation (10) is written in the following symbolic form:

$$E = E(T_u). \quad (11)$$

An iterative procedure is

$$T_u^{m+1} - T_u^m + \lambda E(T_u^m) = 0, \qquad T_u^0 = T^n, \quad (12)$$

where λ is the convergence parameter which must be chosen to be converged and m is the index of iteration. The condition for convergence is obtained by a Fourier analysis [22]. The necessary condition for the solution of Eq. (12) to be stable is

$$\lambda \leqslant \left[\left(\frac{1}{2\,\Delta t}+\frac{2\kappa_i}{\mathrm{MAX}(\Delta r^2, \Delta z^2)}\right)\right]^{-1}, \quad (13)$$

where Δt is a time step and Δr and Δz are a space-variable increment and time-variable increment, respectively.

In order to improve the convergence, the iterative procedure described above can be modified by using the values of the unknowns at iteration $m+1$ in Eq. (12) as soon as they are computed. So this procedure becomes a Gauss–Seidel technique.

The numerical algorithm becomes:

(1) the temperature distribution in the solid, the liquid, and the solid–liquid interface shape are given as the initial conditions;

(2) the temperature profile at the walls moves at the velocity of V_0 and the new temperature at walls is given;

(3) compute the new interface line g^{n+1} using Eq. (9) as below:

$$g^{n+1} = g^n + \Delta t \cdot (1+g_r^2)\left(-K_L \left.\frac{-r_\eta T_\xi + r_\xi T_\eta}{J_0}\right|_L + K_S \left.\frac{-r_\eta T_\xi + r_\xi T_\eta}{J_0}\right|_S\right)^n; \quad (14)$$

(4) transform from the physical plane to the computational plane by the use of the interface line at the time level $n+1$;

(5) solve Eq. (7) under an adequate time and space increment and obtain the temperature at the $n+1$ time step;

(6) calculate the moving velocity of the grid points, that is, $(\partial z/\partial t)^{n+1}$ and $(\partial r/\partial t)^{n+1}$, using the above results;

(7) repeat the procedure (2).

It is noted that the approximation of the first derivative $g(r, t)$ on r needs the most attention. The errors of the approximation cause the instability. For high accuracy, we use the B-spline function described in [17]. The B-spline function is also very usable for the case of the unsteady solidification problem.

RESULTS AND DISCUSSION

The mesh is shown in Fig. 2. The model is calculated for a 15×40 grid. The mini-supercomputer C1-120 (Convex) is used to calculate all cases. The time for one calculation takes about three days when the time-variant increment, Δt, and the growth time are taken as 0.1 s and typically 2×10^6 s, respectively. The values used for the calculation are listed in Table I.

The values of the delay time, τ, defined by Eq. (15), are calculated for two different kinds of the time-variant increment, Δt. When Δt is 0.2, the ratio, τ/τ_0 becomes 1.1, where τ_0 represents the value at $\Delta t = 0.1$. On the other hand, when Δt is 0.4, τ/τ_0 becomes 1.75. So in view of the accuracy, the value of Δt is fixed as 0.1.

The reason for such a long time being required for one

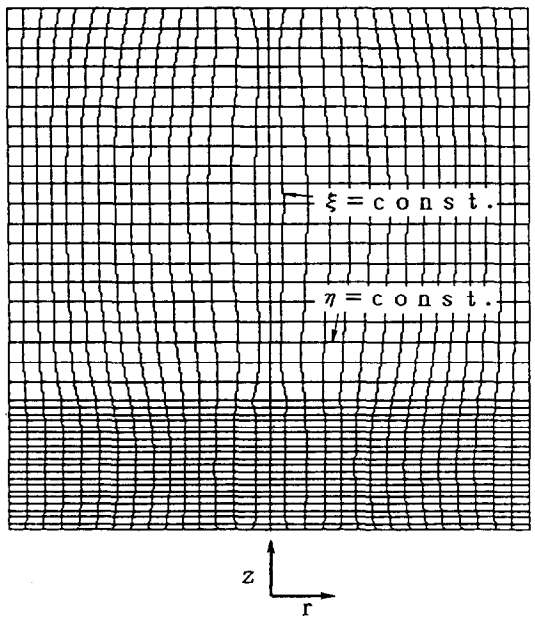

FIG. 2. An example of mesh grid.

calculation is that the program compiled in this study is partially vectorized. If the program is highly tuned and fully vectorized, the time for one calculation will be at least one-fifth shortened.

1. *Comparison with the Analysis of One-Dimensional Unsteady Solidification*

When the width of the ampoule W increases, the side walls acting as the heat sink have little influence on the temperature distribution near the center of the ampoule. Figure 3 displays that with the side walls as the heat sink they only influence the portion near them. In fact, the isothermal lines near the center and the solid–liquid interface are parallel to the r axis. So the solution of the two-dimensional unsteady solidification problem is expected to

TABLE I

Values of Parameters Used in Calculation

Parameter / Figure	k_L/k_S (W/cm · K)	m_L/m_S (K/cm)	W/H (cm)	H_S (cm)	V_0 (cm/s) $\times 10^{-5}$	Vi (cm/s) $\times 10^{-5}$	τ (s) $\times 10^4$
Fig. 3	0.14/0.07	1/2	60/15	2.5	5.0	—	—
Fig. 4a	0.14/0.07	1/2	∞/15	2.5	5.0	—	—
Fig. 5	0.14/0.07	1/2	10/10	2.5	1.0	1.0	4.2
Fig. 6	0.56/0.28	2/4	10/10	2.5	5.0	5.0	0.59
Fig. 9	0.56/0.28	2/4	—	1.0	10.0	—	—

Note. Specific heat, c_L/c_S[/g · K] = 0.42/0.42; Density, ρ_L/ρ_S[g/cm^3] = 5.71/5.17; Latent heat, ΔH[J/g] = 726; Melting temperature, Tm[K] = 1511; Time-variable increment, Δt[s] = 0.1; Height of the ampole, H[cm] = $H_S + H_L$[cm]; Height of solid (initial value), H_S[cm].

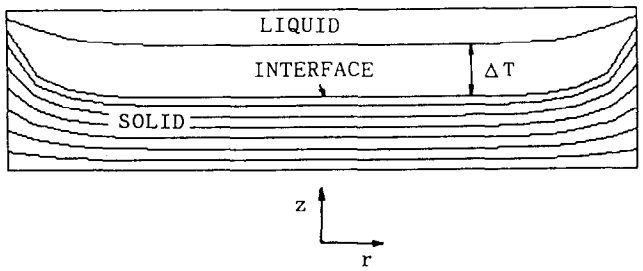

FIG. 3. Illustration of isotherms and solid–liquid interface with a large diameter. $W = 60$ cm, $\Delta T = 4$ K, and the growth time, 1.08×10^5 s.

approach the one-dimensional solution when the width of the ampoule increases. The analytical solution of the one-dimensional unsteady solidification problem is in general obtained more easily than that of the two-dimensional case. So we try the analysis of it and the results are presented in Appendix B.

If some approximations are applied to Eq. (B.14), the analytical solution will be obtained. But here we solve Eq. (B.14) by numerical calculation to be compared with the results in two dimensions. According to the numerical method of ordinary differential equations, for example, Milne's method [23], we calculate Eq. (B.14) and obtain the crystal growth length. Values for the calculation are listed in Table I. Figure 4 shows the dependence of the growth length on the growth time. It is found that the crystal growth length at $r = 0$ in the two-dimensional case is in very good agreement with that in the one-dimensional case. So we conclude that the present method is also reliable in the case of the two-dimensional unsteady solidification problem.

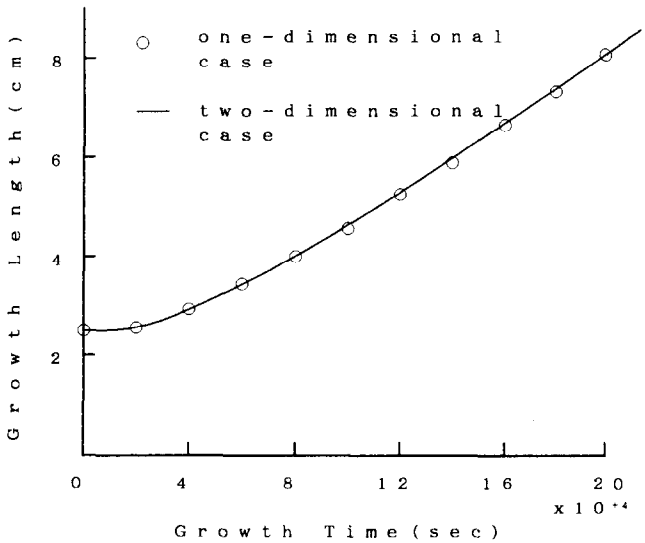

FIG. 4. Comparison with the calculation results in one dimension and that in two-dimensions: (a) one-dimensional solution; (b) two-dimensional solution at $r = 0$.

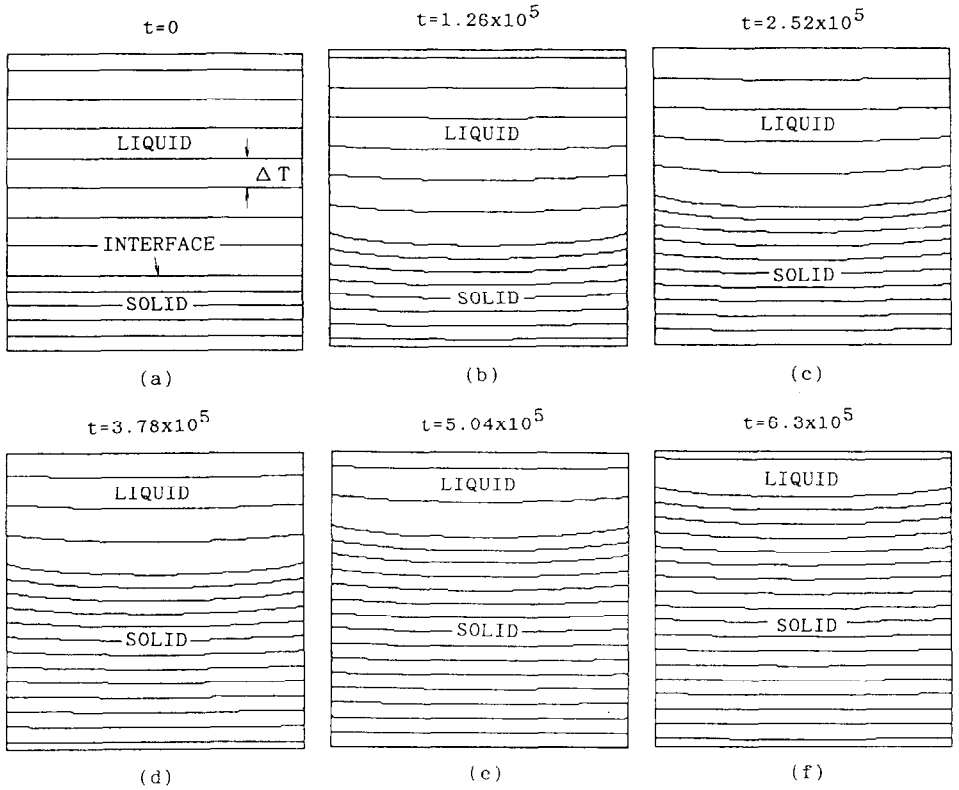

FIG. 5. Illustrations of the dependence of the solid–liquid interface and the isotherms on the growth time. $V_0 = 1.0 \times 10^{-5}$ (cm/s), $\Delta T = 1$ K, the growth time t s.

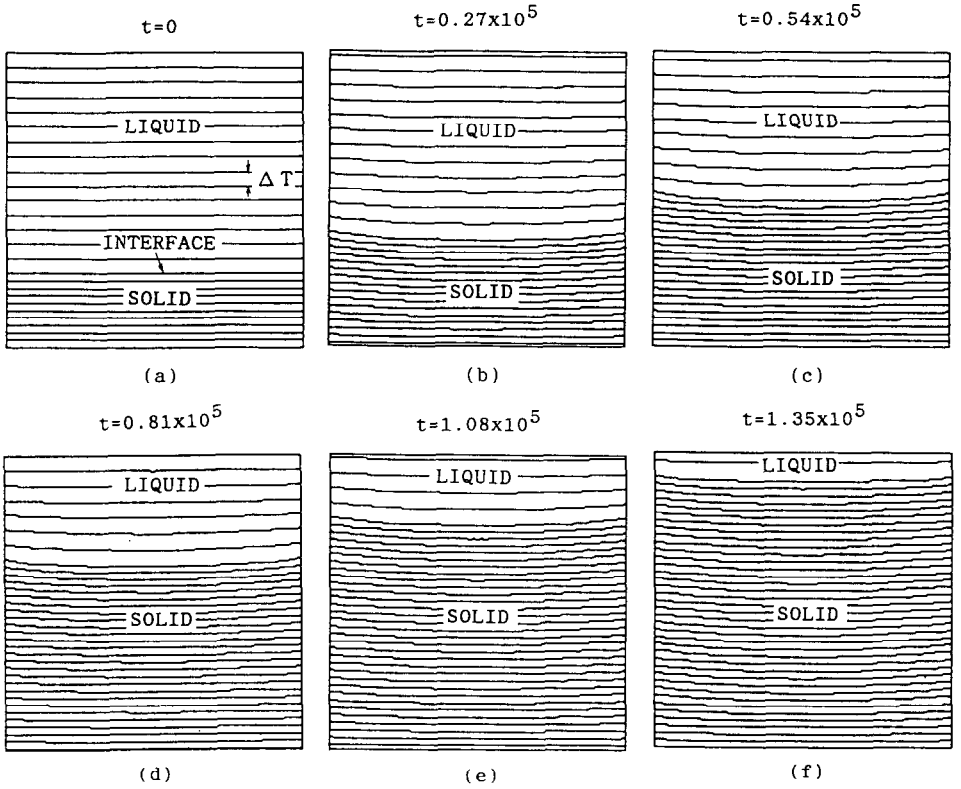

FIG. 6. Illustrations of the dependence of the solid–liquid interface and the isotherms on the growth rate. $V_0 = 5.0 \times 10^{-5}$ (cm/s), $\Delta T = 1$ K, the growth time t s.

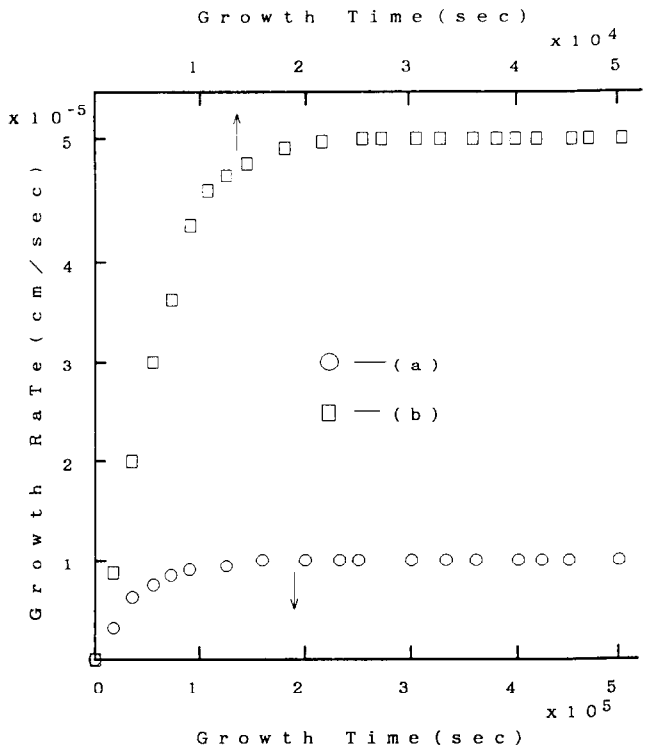

FIG. 7. Dependence of the growth rate at $r = 0$ on the growth time in Figs. 5 and 6: (a) growth rates obtained from Fig. 5; (b) growth rates obtained from Fig. 6.

2. *Unsteady Solidification Process*

The unsteady solidification processes are shown in Fig. 5 and Fig. 6. Values for the calculations are listed in Table I. The initial conditions of the interface shape and the temperature distribution which are solved by the method in [17] are given and the results are shown in Figs. 5a and 6a. The dependence of the growth rate on time is shown in Fig. 7. It is found that the growth curve in Fig. 7 has a constant growth rate after the increase of the growth rate. This constant growth rate is equal to the moving velocity of the temperature profile, V_0, as shown Table I. So the interface shape is independent of time in this portion.

The growth rate calculated at $r = 0$ is approximated by the function

$$V = Vi[1 - e^{-(t/\tau)^f}], \tag{15}$$

where $Vi = V_0$.

This equation is chosen from the following reasons:

(a) We aim at seeking the transient response of the solid–liquid interface to the decrease of the temperature at walls. On the analogy of the damped oscillation [24], we guess, the latent heat and finite heat transfer rate act as the damping force in the equation of the damped oscillation and cause the delay of response. The type of solution for the damped oscillation has the form of $\exp(-\delta t)$, where δ is an attenuation constant.

(b) The derivative of V on t, dV/dt is equal to nil when $t = 0$ and $t > \tau$ as shown in Fig. 8. This means that the curve of the growth rate, V, must have one point of inflection. Therefore, it concludes that the value of f should be greater than one.

We determine Vi and τ by using the least squares method when $f = 1.2$. The results are shown in Table I. Figure 8 shows that Eq. (15) gives a good approximation. Vi is equal to the moving velocity of the temperature profile, V_0, which is equal to the growth rate at $r = W/2$. τ is the delay time which represents the necessary time for the growth rate to approach a constant value. Therefore, after the delay time, the crystal growth condition attains the steady solidification. Wang and Witt [5] reported the similar phenomenon of the growth rate, using the Bridgman growth of gallium-doped germanium. So we conclude that the crystal growth rate is described by the delay time and the moving velocity of the temperature profile.

The dependence of the delayed time τ on the parameters is reported in detail elsewhere [25]. One of the conclusions in Ref. [25] is described as

$$\tau \propto \frac{\rho \Delta HR}{mk}, \tag{16}$$

where m is the temperature gradient at the walls and k is the thermal conductivity. In view of the response of the solid–liquid interface to the decrease in the temperature at the walls, Eq. (16) is reasonable, qualitatively. For example, a fast response is expected to be obtained when the liquid and the solid have high thermal conductivities. As shown in Eq. (16), τ becomes a small value in such a case.

Figure 9 shows the growth process for a complicated shape of the ampoule. The parameters used for the calculation are listed in Table I. Such an ampoule is often used for the small seed crystals. It is difficult to calculate the transient

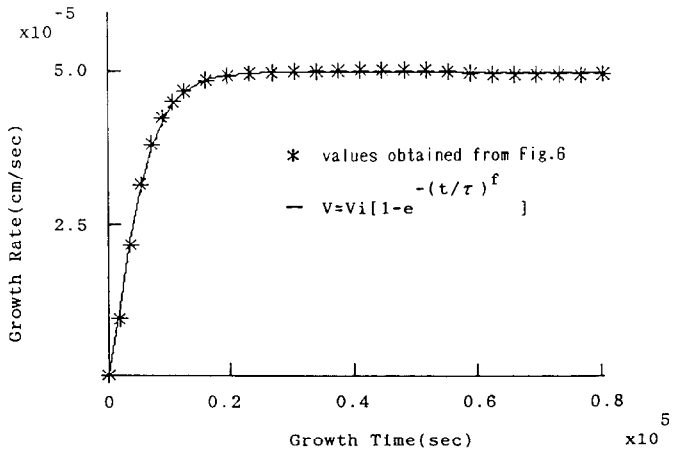

FIG. 8. Fitting of Eq. (15) to the growth rate at $= 0$ in Fig. 7a.

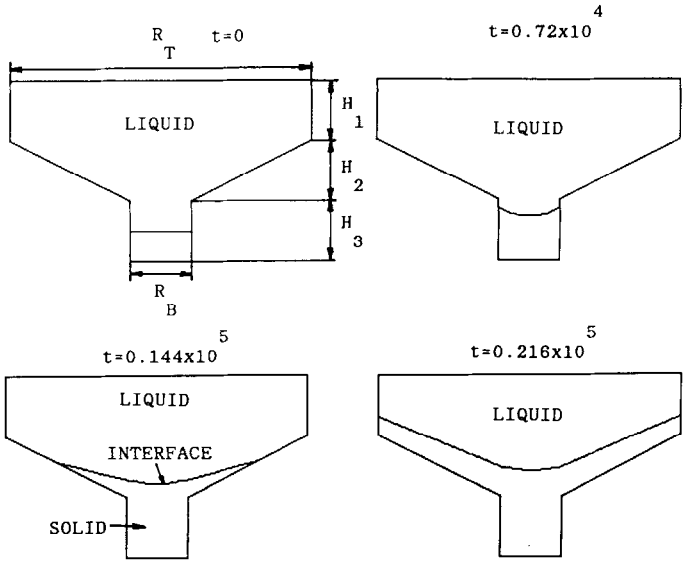

FIG. 9. The growth process with a complicated shape of ampoule: $H_1 = 2.0$ cm, $H_2 = 2.0$ cm, $H_3 = 2.0$ cm, $R_B = 2.0$ cm, $R_T = 10.0$ cm.

growth by use of the transformation proposed by Duda [8] and Saitoh [9]. However, the transformation in Eq. (5) can treat the ampoule easily if the coordinates of the boundary are given. Moreover, we extend the numerical method in this study to the instability of the solid–liquid interface with a solute element [26].

CONCLUSIONS

1. We present a numerical method to calculate the unsteady solidification problem using the boundary-fitted coordinate system.

2. The numerical result for the two-dimensional case with a large diameter of solid is in good agreement with the analysis of the one-dimensional unsteady solidification problem.

3. It is found that the growth rate is described by the delayed time and the moving velocity of the temperature profile at the side walls. After the delay time, the interface shape is unchanged; that is, the interface shape attains the steady state.

APPENDIX A: The Elliptic Generation System in Cylindrical Coordinates with an Axisymmetrical Axis

From the definition of a Jacobian, J [27], we have

$$J = \begin{vmatrix} x_\xi & x_\eta & x_\zeta \\ y_\zeta & y_\eta & y_\zeta \\ z_\xi & z_\eta & z_\zeta \end{vmatrix}, \tag{A.1}$$

where (ξ, η, ζ) are the curvilinear coordinates.

The transformation from the cartesian coordinates to the cylindrical coordinates is made by substituting $x = r\cos\theta$ $y = r\sin\theta$, and $z = z$ into Eq. (A.1):

$$J = r[(r_\xi\theta_\eta - r_\eta\theta_\xi)\, z_\zeta + (r_\xi\theta_\zeta - r_\zeta\theta_\xi)\, z_\eta + (r_\eta\theta_\zeta - r_\zeta\theta_\eta)\, z_\xi]. \tag{A.2}$$

The covariant metric tensor metric tensor g_{ij} is obtained in the same way as described above:

$$\begin{aligned} g_{11} &= r_\xi^2 + r^2\theta_\xi^2 + z_\xi^2, \\ g_{12} &= r_\xi r_\eta + r^2\theta_\xi\theta_\eta + z_\xi z_\eta, \\ g_{13} &= r_\xi r_\zeta + r^2\theta_\xi\theta_\zeta + z_\xi z_\zeta, \\ g_{22} &= r_\eta^2 + r^2\theta_\eta^2 + z_\eta^2, \\ g_{33} &= r_\zeta^2 + r^2\theta_\zeta^2 + z_\zeta^2, \\ g_{23} &= r_\eta r_\zeta + r^2\theta_\eta\theta_\zeta + z_\eta z_\zeta. \end{aligned} \tag{A.3}$$

The following relationships are obtained by taking the partial derivatives of $x = r\cos\theta$ on x and those of $y = r\cos\theta$ on y,

$$\begin{aligned} r_x &= \cos\theta, \qquad \theta_x = -\sin\theta/r, \\ r_y &= \sin\theta, \qquad \theta_y = \cos\theta/r. \end{aligned} \tag{A.4}$$

We have, from the chain-rule and Eq. (A.4),

$$\begin{aligned} \xi_r &= \xi_x\cos\theta + \xi_y\sin\theta, \\ \xi_\theta &= r(\xi_y\cos\theta - \xi_x\sin\theta). \end{aligned} \tag{A.5}$$

Using the definitions of ξ_x, ξ_y, ξ_z, Eqs. (A.4) and (A.5), we have

$$\begin{aligned} \xi_r &= r(\theta_\eta z_\zeta - \theta_\zeta z_\eta)/J \\ \xi_\theta &= r(r_\zeta z_\eta - r_\eta z_\zeta)/J \\ \xi_z &= r(r_\eta\theta_\zeta - r_\zeta\theta_\eta)/J; \end{aligned} \tag{A.6}$$

η_{xi} and ζ_{xi} are also derived in the same way.

In the axisymmetrical case, we have

$$J = r(r_\xi z_\zeta - r_\zeta z_\xi), \tag{A.7}$$

$$g_{11} = r_\xi^2 + z_\xi^2, \quad g_{12} = 0, \quad g_{13} = r_\xi r_\zeta + z_\xi z_\zeta, \quad g_{22} = r^2, \quad g_{23} = 0, \quad g_{33} = r_\zeta^2 + z_\zeta^2, \tag{A.8}$$

$$\xi_r = rz_\zeta/J, \quad \xi_z = -rr_\zeta/J, \quad \zeta_r = -rz_\xi/J, \quad \zeta_z = rr_\xi/J. \tag{A.9}$$

The expression of the Laplacian of scalar function A is

$$\nabla^2 A = \sum_{i,j=1} g^{ij} A_{\xi^i \xi^j} + \sum_{j=1} \nabla^2 \xi^j A_{\xi^j}, \tag{A.10}$$

where $\xi^1 = \xi$, $\xi^2 = \eta$, and $\xi^3 = \zeta$;

$$g^{il} = (g_{jm} g_{kn} - g_{jn} g_{km})/J^2, \quad \text{with} \quad (i, j, k) \text{ and } (l, m, n) \text{ cyclic.} \tag{A.11}$$

Substituting Eq. (A.8) into Eq. (A.11), we obtain

$$\begin{aligned} g^{11} &= r^2(r_\zeta^2 + z_\zeta^2)/J^2, \quad & g^{22} &= 1/r^2, \\ g^{33} &= r^2(r_\xi^2 + z_\xi^2)/J^2, \quad & g^{12} &= 0, \\ g^{13} &= -r^2(r_\xi r_\zeta + z_\xi z_\zeta)/J^2, \quad & g^{23} &= 0. \end{aligned} \tag{A.12}$$

Equation (A.10) can be written by using Eq. (A.12),

$$\nabla^2 A = g^{11} A_{\xi\xi} + 2g^{13} A_{\xi\zeta} + g^{33} A_{\zeta\zeta} + \nabla^2 \xi A_\xi + \nabla^2 \zeta A_\zeta. \tag{A.13}$$

The Laplacians of the cylindrical and the curvilinear coordinates are expressed by

$$\begin{aligned} \nabla^2 r &= 1/r, \quad & \nabla^2 z &= 0, \\ \nabla^2 \xi &= P, \quad & \nabla^2 \zeta &= Q. \end{aligned} \tag{A.14}$$

Substituting Eq. (A.14) into Eq. (A.13), we have the elliptic generation system in cylindrical coordinates with the symmetrical axis, z:

$$\begin{aligned} \alpha r_{\xi\xi} - 2\beta r_{\xi\zeta} + \gamma r_{\zeta\zeta} + P r_\xi + Q r_\zeta &= 1/r, \\ \alpha z_{\xi\xi} - 2\beta z_{\xi\zeta} + \gamma z_{\zeta\zeta} + P z_\xi + Q z_\zeta &= 0, \end{aligned} \tag{A.15}$$

$$\begin{aligned} \alpha &= (r_\zeta^2 + z_\zeta^2)/J_0^2, \quad & \beta &= (r_\xi r_\zeta + z_\xi z_\zeta)/J_0^2, \\ \gamma &= (r_\xi^2 + z_\xi^2)/J_0^2, \quad & J_0 &= r_\xi z_\zeta - r_\zeta z_\xi. \end{aligned} \tag{A.16}$$

APPENDIX B: ONE-DIMENSIONAL UNSTEADY SOLIDIFICATION PROBLEM WITH A FINITE LENGTH

The governing equations are given as

$$\frac{\partial T}{\partial t} = \kappa_i \frac{\partial^2 T}{\partial x^2} \quad (i = \text{L or S}) \tag{B.1}$$

$$-k_L \left.\frac{\partial T}{\partial x}\right|_L + k_S \left.\frac{\partial T}{\partial x}\right|_S = \Delta H \rho \frac{dq}{dt}, \tag{B.2}$$

$$T(x, 0) = T_0(x), \quad \text{at} \quad t = 0 \tag{B.3}$$

$$T(0, t) = -T_1 - v_S t, \quad \text{at} \quad x = 0 \tag{B.4}$$

$$T(q, t) = 0, \quad \text{at} \quad x = q \tag{B.5}$$

$$T(h, t) = T_2 - v_L t, \quad \text{at} \quad x = h, \tag{B.6}$$

where q [cm] is a position of the solid–liquid interface, h [cm] is a height of the ampoule, $T_0(x)$ is the initial temperature distribution, T_i is the initial temperature and v_i [K/s] is the cooling rate. $T(x, t)$ described above is replaced by $T(x, t) - Tm$.

Using Eq. (B.3) and the Laplace transform $\bar{T}(x, s)$ of $T(x, t)$ for Eq. (B.1), we have over the interval $0 \leqslant x \leqslant q$,

$$\frac{d^2 \bar{T}}{dt^2} = (s\bar{T} - T_0(x))/\kappa_i. \tag{B.7}$$

Then, using Eq. (B.4) and the Laplace transform $T'(z, s)$ of $\bar{T}(x, s)$ for Eq. (B.7), we have

$$T' = -\left(\frac{T_1}{s} + \frac{v_S}{s^2}\right)\frac{z}{z^2 - s/\kappa_S} + \frac{\bar{T}_x(0, s)}{z^2 - s/\kappa_S} - \frac{T'_0(z)}{\kappa_S(z^2 - s/\kappa_S)}. \tag{B.8}$$

By the use of inversion of the Laplace transform and Eq. (B.5), $\bar{T}(x, s)$ has the form

$$\begin{aligned} \bar{T}(x, s) = &-\left(\frac{T_1}{s} + \frac{v_S}{s^2}\right)\cosh(s/\kappa_S)^{1/2} x \\ &+ \left(\frac{T_1}{s} + \frac{v_S}{s^2}\right)\frac{\cosh(s/\kappa_S)^{1/2} q}{\sinh(s/\kappa_S)^{1/2} q} \\ &\times \sinh(s/\kappa_S)^{1/2} x + (1/\kappa_S)\int_0^x T_0(\xi) \\ &\times \frac{\sinh(s/\kappa_S)^{1/2}\,\xi\,\sinh(s/\kappa_S)^{1/2}(q - x)}{(s/\kappa_S)^{1/2}\sinh(s/\kappa_S)^{1/2} q} d\xi \\ &+ (1/\kappa_S)\int_x^q T_0(\xi) \\ &\times \frac{\sinh(s/\kappa_S)\,x\,\sinh(s/\xi_S)^{1/2}(q - \xi)}{(s/\kappa_S)^{1/2}\sinh(s/\kappa_S)^{1/2} q} d\xi. \end{aligned} \tag{B.9}$$

Moreover, applying the residue theorem to Eq. (B.9), we have $T(x, t)$,

$$\begin{aligned} T(x, t) = &-T_1 - v_S\left(t + \frac{x^2}{2\kappa_S}\right) + \frac{T_1 x}{q} \\ &+ \frac{v_S x}{q}\left(t + \frac{q^2}{3\kappa_S} + \frac{x^2}{6\kappa_S}\right) \\ &+ \sum_{n=1}^{\infty} \frac{2T_1 \sin(n\pi x/q)}{n\pi} e^{-(n\pi/q)^2 \kappa_S t} \\ &- \sum_{n=1}^{\infty} \frac{2v_S q^2}{(n\pi)^3 \kappa_S} \sin\frac{n\pi}{q} x e^{-(n\pi/q)^2 \kappa_S t} \\ &+ \frac{2}{q}\sum_{n=1}^{\infty} \sin(n\pi x/q)\int_0^q T_0(\xi) \\ &\times \sin(n\pi\xi/q)\, d\xi e^{-(n\pi/q)^2 \kappa_S t}. \end{aligned} \tag{B.10}$$

In the same way, we obtain, over the interval $q \leqslant x \leqslant h$,

$$T(x,t) = T_2 - v_L\left[t + \frac{(h-x)^2}{2\kappa_L}\right] + \frac{T_2(h-x)}{h-q} + \frac{v_L(h-x)}{h-q}\left[t + \frac{(h-q)^2}{3\kappa_L} + \frac{(h-x)^2}{6\kappa_L}\right] - \sum_{n=1}^{\infty} \frac{2T_2 \sin[n\pi(h-x)/(h-q)]}{n\pi} \times e^{-[n\pi/(h-q)]^2 \kappa_L t} - \sum_{n=1}^{\infty} \frac{2v_L(h-q)^2}{(n\pi)^3 \kappa_L} \sin\frac{n\pi}{h-q}(h-x) \times e^{-[n\pi/(h-q)]^2 \kappa_L t} + \frac{2}{h-q}\sum_{n=1}^{\infty} \sin\frac{n\pi(h-x)}{h-q} \int_0^{h-q} T_0(h-\xi) \times \sin\frac{n\pi\xi}{h-q}\, d\xi e^{-[n\pi/(h-q)]^2 \kappa_L t}. \quad \text{(B.11)}$$

The initial temperature distribution is given as

$$T_0(x) = \begin{cases} m_S(x-q), & 0 \leqslant x \leqslant q, \\ m_L(x-q), & q \leqslant x \leqslant h. \end{cases} \quad \text{(B.12)}$$

where m_S and m_L are the temperature gradient in solid and that in liquid, respectively.

From Eqs. (B.3), (B.4), (B.6), we have

$$T_1 = -m_S q, \qquad T_2 = m_L(h-q). \quad \text{(B.13)}$$

Equations (B.2), (B.10), (B.11), and (B.13) give the growth rate of the crystal,

$$\frac{dq}{dt} = -\frac{k_L}{\rho\, \Delta H}\left[\frac{T_2}{h-q} + \frac{v_L(h-q)}{6\kappa_L} - \frac{v_L t}{h-q} + \sum_{n=1}^{\infty} (-1)^n \frac{2v_L(h-q)}{(n\pi)^2 \kappa_L} e^{-[n\pi/(h-q)]^2 \kappa_L t}\right] + \frac{k_S}{\rho\, \Delta H}\left[\frac{T_1}{q} - \frac{v_S q}{6\kappa_S} + \frac{v_S t}{q} - \sum_{n=1}^{\infty} (-1)^n \frac{2v_S q}{(n\pi)^2 \kappa_S} e^{-(n\pi/q)^2 \kappa_S t}\right]. \quad \text{(B.14)}$$

ACKNOWLEDGMENTS

The first author thanks Dr. M. Kawashima and Dr. E. Kanda of Sumitom Metal Mining Co., Ltd. for their encouragement in this study.

REFERENCES

1. K. M. Kim, A. F. Witt, and H. C. Gatos, *J. Electrochem. Soc.* **121**, 448 (1974).
2. H. U. Walter, *J. Electrochem. Soc.* **123**, 1098 (1976).
3. R. K. Route, M. Wolf, and R. S. Feigelson, *J. Cryst. Growth* **70**, 379 (1984).
4. G. Muller, G. Neumann, and W. Weber, *J. Cryst. Growth* **70**, 78 (1984).
5. C. A. Wang, A. F. Witt, and J. R. Carruthers, *J. Cryst. Growth* **66**, 299 (1984).
6. H. M. Ettouney and R. A. Brown, *J. Cryst. Growth* **58**, 313 (1982).
7. R. A. Brown, *AIChE J.* **34**, 881 (1988).
8. J. L. Duda, M. F. Malone, and R. H. Notter, *Int. J. Heat Transfer* **18**, 901 (1975).
9. T. Saitoh, *ASME J. Heat Transfer* **100**, 294 (1978).
10. W. L. Oberkamp, *Int. J. Numer. Methods Eng.* **10**, 211 (1976).
11. N. Zabaras, *Int. J. Numer. Methods Eng.* **29**, 1569 (1990).
12. M. A. Albert and K. O'Neill, *Int. J. Numer. Methods Eng.* **23**, 591 (1986).
13. J. M. Sullivan, D. R. Lynch, and K. O'Neill, *J. Comput. Phys.* **69**, 81 (1987).
14. N. Zabaras and S. Mukherjee, *Int. J. Numer. Methods Eng.* **24**, 1879 (1987).
15. M. J. Crochet, F. T. Geyling, and J. J. van Schaftingen, *Int. J. Num. Methods Fluids* **7**, 29 (1987).
16. B. Roux and H. B. Hadid, *J. Cryst. Growth* **97**, 201 (1989).
17. M. Saitou, E. Kanda, and M. Kawashima, *J. Comput. Phys.*, appear.
18. M. Saitou, E. Kanda, and M. Kawashima, *J. Jpn. Soc. Simul. Tech.* **9**, 47 (1990).
19. M. Saitou and H. Hirata, to be prepared for submission.
20. J. Crank, *Free and Moving Boundary Problems* (Oxford Sci. London, 1984), p. 18.
21. R. Peyret and T. D. Taylor, *Computational Methods for Fluid Flow* (Springer-Verlag, New York/Berlin, 1982), p. 168.
22. P. J. Roache, *Computational Fluid Dynamics* (Hermosa, Albuquerque, NM, 1976).
23. C. F. Gerald, *Applied Numerical Analysis* (Addison–Wesley, Reading, MA, 1970).
24. A. P. French, *Vibration and Waves* (MIT, Cambridge, MA, 1971).
25. M. Saitou and A. Hirata, *J. Cryst. Growth*, to be submitted.
26. M. Saitou and A. Hirata, *J. Cryst. Growth*, to be submitted.
27. J. F. Thompson, Z. U. A. Warsi, and C. W. Mastin, *Numerical Grid Generation* (North-Holland, Amsterdam, 1985).